21. Local zones of higher respiratory activity may be important, however, as evidenced by higher levels of the respiratory enzyme cytochrome oxidase in the subsets of cells with nitrogenase than in those without (*40*). Deployment of oxygen and reactive oxygen species detoxification systems (such as Mehler, thioredoxin peroxidases, and catalase) also aid in providing a microanaerobic environment around cells fixing nitrogen. Colony formation may further reduce ambient oxygen concentrations (*5, 8*), enabling the higher N_2 fixation rates (per unit of chlorophyll a) observed in colonies as compared to single trichomes (*41*).
22. In mature heterocysts, PSI is the only active photosynthetic reaction center and is important in providing the extra ATP for N_2 fixation through cyclic electron transport. In *Trichodesmium*, high Mehler activity has also previously been invoked in supplying ATP (*42, 43*).
23. Antibodies to D1 fragments and to dinitrogenase reductase raised in rabbits were conjugated to fluorescent probes Alexa 488 and Alexa 568, respectively (Molecular Probes) and labeled sequentially (nitrogenase followed by D1) in cells fixed in 100% ethanol and permeabilized with 0.5% dimethyl sulfoxide in phosphate buffer. Samples were viewed on a confocal laser microscope (Zeiss LSM410) at 488/528 nm and 568/600 to 620 nm bandpass excitation/emission for the D1 and nitrogenase, respectively. The results obtained for cultures grown in several conditions and at several points during the diel cycle show that D1 occurs in most cells in a trichome and co-occurs in the same cells as nitrogenase.
24. Z. Krupa, G. Öquist, P. Gustafsson, *Plant Physiol.* **93**, 1 (1990).
25. *Trichodesmium* colonies were stained with 3,3-diaminobenzidine (DAB), which polymerizes, in the presence of peroxidases, with intracellular H_2O_2 produced by reduction of oxygen in PSI, to form brown deposits (*44*). The final concentration of DAB used was 1 mg/ml. No external peroxidases were added, indicating the presence of active peroxidases involved in the antioxidative pathways [Web fig. 2 (*19*)]. Negative controls of dark-incubated *Trichodesmium* trichomes showed low DAB staining throughout the trichomes.
26. Trichomes were filtered, embedded in 1% agarose (melting point 25°C) in sea water, and placed in a cellophane-sealed thermostated chamber pumped through with medium (100 ml min^{-1} at 25°C, saturated with air). To reduce artifacts caused by handling, fresh samples were prepared for each time point. Samples were viewed with a microscope for two-dimensional measurements of in vivo chlorophyll fluorescence kinetics (*45*). Measurements were done with 30-μs flashes of nonactinic measuring light, 1000 μmol of quanta m^{-2} s^{-1} of actinic light, and 10,000 μmol of quanta m^{-2} s^{-1} saturating multiturnover flashes. Fluorescence kinetics were measured simultaneously on 300 × 400 pixels.
27. A circadian pattern temporally separates the abundance of mRNA for nifH (nitrogenase), psbA (encoding for PSII) and psaB (encoding for PSI) in *Trichodesmium* strain IMS101 (*46, 47*).
28. In *Trichodesmium*, high external concentrations of molecular oxygen affect nitrogenase activity within ~15 min (*48*), whereas Western and Northern blots of nitrogenase and nifH (*49*) revealed that the enzyme and transcript levels are not much affected 2 hours after addition of DCMU and DBMIB, indicating that the loss of activity is not due to the loss of the enzyme but rather to a posttranslational inactivation of the enzyme by oxygen.
29. In most cyanobacteria, dark respiration rates are generally <10% of the gross oxygen evolution rates (*50*). In *Trichodesmium*, dark respiration ranged from 13 to 46% of the maximum gross oxygen evolution rate, with a mean of 23% and consisting, in the dark, of approximately 30% of the absolute magnitude of maximal gross photosynthesis. Moreover, at low light intensities (typical of those found for depth-adapted populations or cultured populations), more oxygen was consumed than evolved (*51, 52*).
30. Phylogenetic analyses suggest a single ancestral origin for the catalytic subunits of the enzyme complex responsible, namely nitrogenase (*53*).
31. P. G. Falkowski, *Nature* **387**, 272 (1997).
32. J. P. Zehr, M. T. Mellon, S. Zani, *Appl. Environ. Microbiol.* **64**, 3444 (1998).
33. C. P. Wolk, A. Ernst, J. Elhai, in *The Molecular Biology of Cyanobacteria*, D. E. Bryant, Ed. (Kluwer Academic, Dordrecht, Netherlands, 1994), pp. 769–823.
34. B. K. Burgess, D. J. Lowe, *Chem. Rev.* **96**, 2983 (1996)
35. Z. Kolber, O. Prašil, P. G. Falkowski, *Biochim. Biophys. Acta* **1367**, 88 (1998).
36. G. H. Krause, E. Weis, *Annu. Rev. Plant Physiol. Plant Mol. Biol.* **42**, 313 (1991).
37. D. Campbell *et al.*, *Microbiol. Mol. Biol. Rev.* **62**, 667 (1998).
38. P. G. Falkowski, J. A. Raven, *Aquatic Photosynthesis* (Blackwell Science, Malden, MA, ed. 1, 1997).
39. M. Hirano, K. Satoh, S. Katoh, *Photosyn. Res.* **1**, 149 (1980).
40. B. Bergman *et al.*, *Appl. Environ. Microbiol.* **59**, 3239 (1993).
41. R. M. Letelier, D. M. Karl, *Aquatic Microbiol Ecol.* **15**, 265 (1998).
42. T. M. Kana, in *Marine Pelagic Cyanobacteria: Trichodesmium and Other Diazotrophs*, E. J. Carpenter, Ed. (Kluwer Academic, Dordrecht, 1992), pp. 29–41.
43. ———, *Limnol. Oceanogr.* **38**, 18 (1993).
44. H. Thordal-Christensen *et al.*, *Plant J.* **11**, 1187 (1997).
45. H. Küpper, I. Šetlik, M. Trtilek, L. Nedbal, *Photosynthetica* **38**, 553 (2000).
46. Y. B. Chen *et al.*, *J. Bacteriol.* **180**, 3598 (1998).
47. ———, *Plant Mol. Biol.* **41**, 89 (1999).
48. P. Lundgren, Y. Gerchman, unpublished data.
49. I. Berman-Frank *et al.*, unpublished data.
50. J. C. P. Matthijs, H. J. Lubberdin, in *Biochemistry of the Algae and Cyanobacteria, Proc. Phytochem. Soc. Eur.* (Clarendon, 1988) pp. 131-145.
51. T. Roenneberg, E. J. Carpenter, *Mar. Biol.* **117**, 693, (1993).
52. E. J. Carpenter, T. Roenneberg, *Mar. Ecol. Prog. Ser.* **118**, 267 (1995).
53. J. P. Zehr, E. J. Carpenter, T. A. Villareal, *Trends Microbiol.* **8**, 68 (2000).

54. We thank D. Capone, E. Carpenter, and the captain and crew of the R/V *Ewing* for enabling the field study; R. Dotson for setting up the continuous flow to the FRR fluorometer; K. Bateman (Stockholm University) and K. Wyman (Rutgers University) for technical assistance; J. Waterbury (Woods Hole Oceanography Institute) for providing axenic cultures, lab space, invaluable help, and ideas; P. Ludden (University of Wisconsin), S. Nordlund (Stockholm University), and A. Matoo (U.S. Department of Agriculture) for their gift of antibodies; O. Prašil, I. Šetlik, and the Microbiological Institute, Trebon, for hosting I.B.-F. [Czech (CZ)-NSF grant ME379 and Ministry of Education of the Czech Republic grant MSM 12310001] and providing access to the kinetic microscope, which was built in cooperation with Photon Systems Instruments, Czech Republic. Supported through grants to P.F. from the U.S. Department of Energy Office of Science program for Research on Ocean Carbon Sequestration, the Center for Bioinorganic Chemistry (Princeton University), NASA Earth System Science Program; to B.B. from the Swedish Foundation for International Cooperation in Research and Higher Education and the Swedish Natural Science Research Council (SIDA/SAREC); and to H. K. from Studienstiftung des Deutschen Volkes.

5 July 2001; accepted 3 October 2001

Tumor Therapy with Targeted Atomic Nanogenerators

Michael R. McDevitt,[1] Dangshe Ma,[1] Lawrence T. Lai,[1] Jim Simon,[2] Paul Borchardt,[1] R. Keith Frank,[2] Karen Wu,[1] Virginia Pellegrini,[1] Michael J. Curcio,[1] Matthias Miederer,[1] Neil H. Bander,[3] David A. Scheinberg[1]*

A single, high linear energy transfer alpha particle can kill a target cell. We have developed methods to target molecular-sized generators of alpha-emitting isotope cascades to the inside of cancer cells using actinium-225 coupled to internalizing monoclonal antibodies. In vitro, these constructs specifically killed leukemia, lymphoma, breast, ovarian, neuroblastoma, and prostate cancer cells at becquerel (picocurie) levels. Injection of single doses of the constructs at kilobecquerel (nanocurie) levels into mice bearing solid prostate carcinoma or disseminated human lymphoma induced tumor regression and prolonged survival, without toxicity, in a substantial fraction of animals. Nanogenerators targeting a wide variety of cancers may be possible.

Alpha particles are high-energy, high linear energy transfer helium nuclei capable of strong, yet selective, cytotoxicity (*1*). A single atom emitting an alpha particle can kill a target cell (*2*). Monoclonal antibodies conjugated to alpha particle–emitting radionuclides (^{213}Bi and ^{211}At) are starting to show promise in radioimmunotherapy (*3, 4*). The conjugates [^{213}Bi]-HuM195 (*2*) and [^{213}Bi]J591 (*5, 6*) have been used in preclinical models of leukemia and prostate cancer, respectively, and in a phase I human clinical trial, [^{213}Bi]HuM195 was active against leukemia, with no significant toxicity (*3*). Astatine-211–labeled antibodies to tenascin (anti-tenascin) have been used clinically to treat malignant gliomas in humans (*4*) in a phase I trial. For clinical use of ^{213}Bi, we developed a therapeutic dose-level ^{225}Ac/^{213}Bi generator device, approximately 1 cm by 6 cm in size,

[1]Molecular Pharmacology and Therapeutics Program, Memorial Sloan-Kettering Cancer Center, 1275 York Avenue, New York, NY 10021, USA. [2]The Dow Chemical Company, Freeport, TX 77541, USA. [3]Department of Urology, New York Presbyterian Hospital-Weill Medical College of Cornell University, 525 East 68th Street, New York, NY 10021, USA.

*To whom correspondence should be addressed. E-mail: d-scheinberg@ski.mskcc.org

capable of producing alpha particle–emitting atoms for attachment to ligands suitable for human injection (*7, 8*). Despite this improvement, the major obstacle to the widespread use of these drugs remains the short ^{213}Bi half-life (46 min), which limits its delivery to only the most accessible cancer cells.

One solution to these constraints is to deliver the atomic generator to the target cell, allowing production of the atoms that will yield potent alpha emissions at or in the cancer cell. For this process to be successful pharmacologically, the device must possess molecular dimensions. At its ultimate reduction, the device therefore consists of a single ^{225}Ac generator atom attached to the delivery vehicle. Actinium-225 has a 10.0-day half-life and decays via alpha emission through three atoms, each of which also emits an alpha particle (*9, 10*). We developed methods that use bifunctional versions of the chelating moiety DOTA (1,4,7,10-tetraazacyclododecane-1,4,7,10-tetraacetic acid) to stably bind ^{225}Ac to the delivery vehicles, and have described the synthesis, purification, and analyses of the resulting constructs [supplementary note 1 (*11*)].

The stability of an ^{225}Ac-DOTA-antibody construct was determined in vitro under conditions similar to those expected in vivo. The [^{225}Ac]DOTA-HuM195 construct was compared with [^{177}Lu]DOTA-HuM195 in 100% human serum, 100% mouse serum, and 25% human serum albumin at 37°C for 15 days. The [^{225}Ac]HuM195 displayed stability similar to the ^{177}Lu analog with less than a 5% loss of ^{225}Ac from the IgG over 15 days [supplementary fig. 1 (*11*)]. The stability data in all three conditions were similar. Importantly, there was no loss of ^{225}Ac to other serum proteins in vivo [supplementary note 2 (*11*)].

We examined the in vitro cytotoxicity of ^{225}Ac constructs specific for HL60 leukemia cells [HuM195 (anti-CD33)]; Daudi and Ramos lymphoma cells [B4 (anti-CD19)]; MCF7 breast carcinoma cells [Herceptin (anti-HER2/neu)]; LNCaP.FGC prostate carcinoma cells [J591 (anti-PSMA)]; and SKOV3 ovarian cancer cells [Herceptin (anti-HER2/neu)] at very small doses of generators (*12*). The median lethal dose (LD_{50}) of the ^{225}Ac constructs ranged from 0.3 to 74 Bq/ml (0.008 to 2 nCi/ml) and were lower than values for corresponding ^{213}Bi alpha particle–emitting antibodies (~7400 Bq/ml) (*2, 5, 13*). Controls at low specific activities (accomplished by adding excess unlabeled antibody) did not show specific binding of the alpha-particle generators to the targets, and were used to represent nonspecific cytotoxicity. The LD_{50} values were 10- to 625-fold higher in the controls using excess unlabeled antibody.

Critical to the success of this generator approach is the retention of the daughter alpha-emitting atoms at or in the target cells. To investigate whether the radionuclidic daughters of target cell–internalized ^{225}Ac constructs were retained intracellularly in vitro, we measured the resulting increase or decrease of the ^{221}Fr and ^{213}Bi daughters relative to secular equilibrium values. The antibodies HuM195, J591, and B4 internalize into HL60, LNCaP, and Daudi cells, respectively, after binding (*2, 5, 14–16*), carrying with them the attached ^{225}Ac radionuclide. Analyses of the internalized generators show that initially there were greater than equilibrium levels of ^{221}Fr and ^{213}Bi daughters present inside the cells (Fig. 1A).

The in vivo biodistribution of the generator constructs and the radionuclidic daughters was determined in mice bearing a LNCaP carcinoma. Approximately 18 and 21% of the injected dose of [^{225}Ac]J591 was localized in the tumor (per g) at 2 and 3 days, respectively. Tumor samples (average ± SD, $n \geq 3$) counted 6 to 12 min after death revealed that ^{221}Fr was 88% ± 9% and ^{213}Bi was 89% ± 2% of the ^{225}Ac secular equilibrium levels of the tumor associated radioactivity (Fig. 1B). These measurements, however, represent a composite value of tumor cell–internalized and surface-bound [^{225}Ac]J591 and its decay daughters. The daughters produced on the tumor cell's outer membrane surface might be transferred away to other sites such as the kidneys and intestine.

To investigate the in vivo therapeutic efficacy of the generator construct [^{225}Ac]J591, we used an intramuscular (i.m.) LNCaP tumor model (*5*) in male nude mice. Serum prostate-specific antigen (PSA) is an important surrogate marker for prostate cancer burden and prognosis in humans (*17*). It can also be used in animal models with prostate cancer cell xenografts (*5, 18*). Rising PSA levels predict the appearance of visible tumor and death. The mice in our experimental groups had mean PSA values of 2 to 5 ng/ml on 10 and 12 days after implantation of tumor. At the time the generator was administered on day 12 or 15, the tumors were characterized histologically as vascularized and encapsulated nodules, each containing tens of thousands of tumor cells (*5*). A single nontoxic (*19*) administration of the generator construct

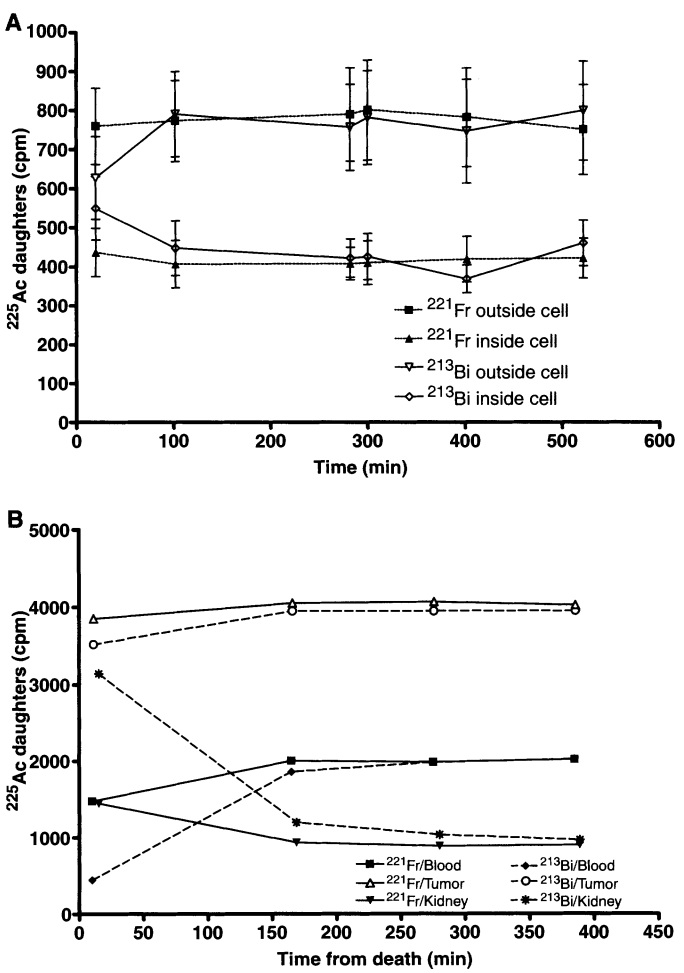

Fig. 1. (**A**) Internalization and retention in vitro of [^{225}Ac]J591/^{213}Bi/^{221}Fr in LNCaP cells. Actinium-225 that was internalized or was outside the cell was determined after a 5-hour period when secular equilibrium was established and the ^{213}Bi and ^{221}Fr curves converge. The radionuclidic decay of ^{225}Ac yields two daughter radionuclides, ^{221}Fr and ^{213}Bi, that can be monitored in these experiments by gamma spectroscopy. Values shown are mean ± SD. LNCaP cells (10^7 cells) were exposed to an antibody-to-antigen excess of [^{225}Ac]J591 at 37°C for 90 min [supplementary note 3 (*11*)]. (**B**) Biodistribution in vivo of [^{225}Ac]J591/^{213}Bi/^{221}Fr in several tissues from one representative mouse. Actinium-225 that was tissue-associated was determined after a 5-hour period when secular equilibrium was established and the ^{213}Bi and ^{221}Fr curves converge. Pharmacological analysis of the two ^{225}Ac daughters was performed in vivo by injecting 12 kBq of [^{225}Ac]J591 or 12 kBq of [^{225}Ac]HuM195 (irrelevant control) intraperitoneally in two groups of male athymic nude mice (n = 12 per group) (Taconic, Germantown, New York) bearing a 3- to 4-week-old LNCaP i.m. tumor xenograft. Mice from each group were killed at days 2 and 3, respectively, and the tumors, blood, and other tissues were removed and immediately counted with a Packard Cobra Gamma Counter using two energy windows [supplementary note 3 (*11*)].

15 days after implantation significantly improved ($P < 0.006$) median survival times of mice relative to mice treated with [^{225}Ac]B4 irrelevant control antibody mixed with unlabeled specific J591 (dual control) or untreated controls [Supplementary fig. 2 (*11*)]. There was no significant difference in survival times between the dual control–treated animals and untreated controls. The median survival time of untreated controls in this model was 33 days ($n = 15$). The mean and median pretherapy PSA values measured on day 12 were not significantly different among the three groups of mice. However, on days 28 and 42, the PSA values of [^{225}Ac]J591-treated animals were significantly lower than the PSA values for the dual control–treated animals and untreated controls [supplementary fig. 3 (*11*)]. There was no significant difference in PSA levels between the dual control–treated animals and untreated controls at either time.

Earlier treatment of mice, on day 12 after LNCaP tumor implantation with a single administration of [^{225}Ac]J591, caused tumor regression and significantly improved ($P < 0.0001$) the median survival times of these mice to 158 days compared to 63 days in the mice treated on day 15 (Fig. 2A). After treatment, PSA levels decreased from pretherapy levels in many of the mice to low and undetectable levels and remained undetectable in 14 animals, of the 39 treated animals; all 39 animals exhibited prolonged survival (Fig. 2B). These mice survived at least 10 months and had no measurable PSA levels or evidence of tumor at the time of death (293 days). Animals treated with unlabeled J591 (0.004 or 0.04 mg) on day 12 after implantation had no prolongation of median survival (37 and 35 days, respectively; $n = 9$). The therapeutic efficacy was dependent on antibody specificity, the administration of the ^{225}Ac-generator, and the delay time between tumor implantation and initiation of treatment.

To determine if other tumor types could be treated with ^{225}Ac-generator constructs, we investigated a disseminated human Daudi lymphoma cell mouse model (*20*), using [^{225}Ac]B4 as the therapeutic agent. Mice were treated 1 day after tumor dissemination with a single administration of specific [^{225}Ac]B4 (three different dose levels), irrelevant control [^{225}Ac]HuM195 (two dose levels), or unlabeled B4. Control mice receiving the irrelevant [^{225}Ac]HuM195 had median survival times from xenograft of 43 days (5.6 kBq) and 36 days (1.9 kBq). Mice receiving 0.003 mg of unlabeled B4 per mouse had a median survival time of 57 days. The mice receiving a single injection of [^{225}Ac]B4 showed dose-related increases in median survival times: 165 days (6.3 kBq), 137 days (4.3 kBq), and 99 days (2.1 kBq) (Fig. 3A). This dose response of [^{225}Ac]B4 was significant ($P = 0.05$). About 40% of mice treated at the highest dose were tumor-free at 300 days, and the experiment concluded on day 310.

We also examined the effect of treatment delay in the disseminated lymphoma model (Fig. 3B). Mice ($n = 15$) that received a single injection of [^{225}Ac]B4 (6.3 kBq) treatment on day 1, 3, or 6 after tumor implantation had a similar prolongation of survival relative to untreated controls (28 or 30 days for controls versus 103, 95, or 108 days for animals treated on days 1, 3, or 6, respectively). Mice ($n = 5$)

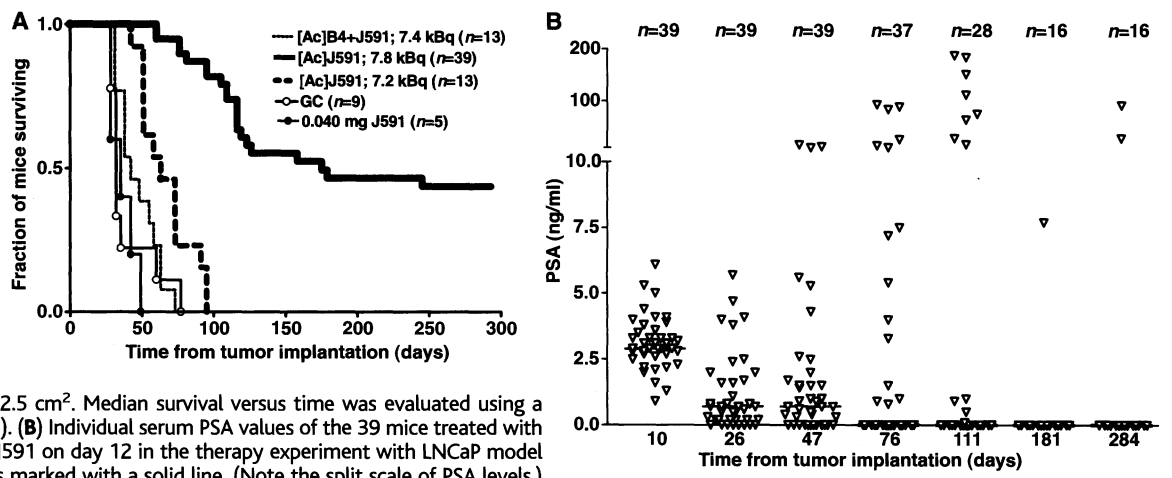

Fig. 2. (**A**) Kaplan-Meier plot showing survival of mice bearing i.m. LNCaP tumor xenografts treated intraperitoneally in several therapy/control experiments. The 39 animals that received 7.8 kBq [^{225}Ac]J591 were treated on day 12, and the 13 animals that received 7.2 kBq [^{225}Ac]J591 were treated on day 15. Animals were killed when tumor area was ≥ 2.5 cm^2. Median survival versus time was evaluated using a log-rank test ($P < 0.0001$). (**B**) Individual serum PSA values of the 39 mice treated with a 7.8 kBq dose of [^{225}Ac]J591 on day 12 in the therapy experiment with LNCaP model (Fig. 2A). The median was marked with a solid line. (Note the split scale of PSA levels.) PSA values were evaluated using an unpaired *t*-test with two-tailed *P* values (95% confidence limit) to analyze differences between study groups.

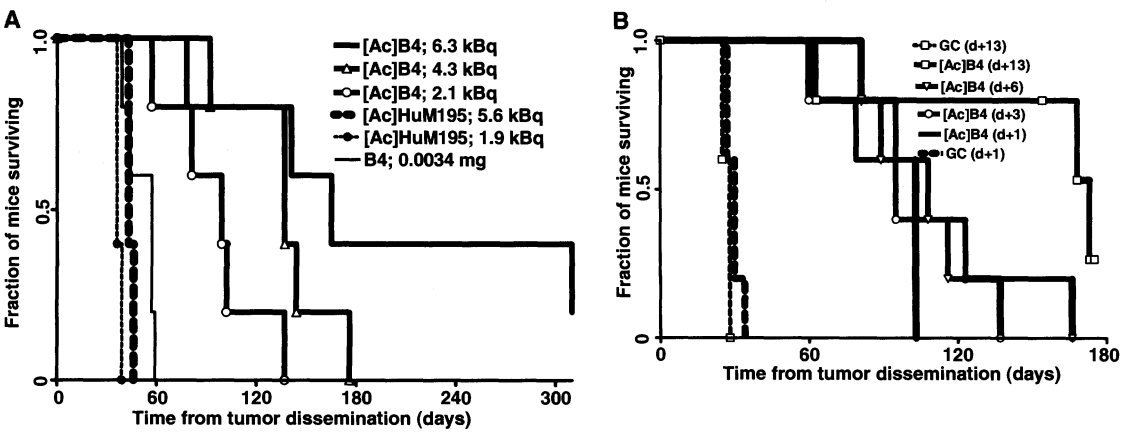

Fig. 3. (**A**) Kaplan-Meier plot showing survival of mice bearing a disseminated Daudi xenograft. In this lymphoma therapy experiment, mice (groups of $n = 5$) were treated 1 day after tumor dissemination via intravenous injection. Animals were monitored for signs of morbidity or hind-leg paralysis, at which time they were killed. Median survival versus time was evaluated using a log-rank test ($P < 0.0001$). (**B**) Kaplan-Meier plot showing survival of mice bearing a disseminated Daudi xenograft. Mice (groups of $n = 5$) were treated with a single 6.3-kBq dose of [^{225}Ac]B4 on days 13, 6, 3, and 1 after intravenous xenograft. Controls were untreated animals with xenografts initiated day 13 or 1. Animals were monitored and statistical analysis was performed as described above ($P < 0.0001$).

that received treatment as late as 13 days after tumor dissemination survived >173 days. Unlabeled B4 was minimally active in mice (n = 5 per group) with median survival of 44 or 40 days for mice treated with 0.002 or 0.20 mg, respectively. Untreated controls (n = 15) had a median survival time of 28 days. Therefore, in this lymphoma model, although specificity and dose level were important factors in efficacy, the delay between tumor dissemination and initiation of treatment was less relevant up to a certain time point, at which it was then inversely related to activity. This observation may be related to the geometry of the emitted radiation of the alpha particle, which may kill a cluster of cells more easily than a single cell.

Previous workers have concluded that therapy with ^{225}Ac-constructs might not be feasible because the constructs are unstable and because the radionuclidic daughters present an untenable pharmacological problem (*21–24*). However, our findings indicate that ^{225}Ac can be used as a safe and potent tumor-selective molecular-sized generator in both established solid carcinomas or disseminated cancers. In part, the enhanced potency of these constructs as compared to the ^{213}Bi analogs can be attributed to the longer half-life (313-fold greater ^{225}Ac half-life) and the four net alpha particles emitted by the ^{225}Ac, but other mechanisms must also be involved, such as more efficient cytotoxicity following intracellular delivery of the generator. Once inside the cell, the geometry of the decay trajectory of the alpha particle favors highly efficient cell killing: each decay must pass through the cell, whereas statistically only 30% of the alpha decays will pass through the cell if the generator is surface bound (*2*). Selection of tumor antigen systems that internalize the ^{225}Ac generator construct help to retain the daughters and therefore lead to enhanced potency; however, internalization is not required for activity.

The development of synthetic methods to yield stable nanogenerator constructs of [^{225}Ac]IgG in useful quantities, and the demonstration of safe, efficacious deployment against murine models of both solid carcinomas and disseminated cancer, using very small doses of isotope, suggest a pathway to widespread clinical use of such targeted drugs. The 10-day half-life of the ^{225}Ac generator constructs would allow the drugs to be manufactured at a central radiopharmacy and shipped throughout the world. Because of the extraordinary potency of ^{225}Ac generators, little radioactivity [possibly sub-MBq (mCi)] would be required for therapeutic human use, allowing for economical outpatient use and safety. In addition, the longer half-life of ^{225}Ac may allow better penetration of larger tumors.

References and Notes

1. J. L. Humm, L. M. Chin, *Radiat. Res.* **134**, 143 (1993).
2. T. N. Nikula *et al.*, *J. Nucl. Med.* **40**, 166 (1999).
3. J. G. Jurcic *et al.*, *Blood* **90**, 504a (1997).
4. M. R. Zalutsky, G. Vaidyanathan, *Curr. Pharm. Des.* **6**, 1433 (2000).
5. M. R. McDevitt *et al.*, *Cancer Res.* **60**, 6095 (2000).
6. Å. M. Ballangrud *et al.*, *Cancer Res.* **61**, 2008 (2001).
7. M. R. McDevitt, R. D. Finn, G. Sgouros, D. Ma, D. A. Scheinberg, *Appl. Radiat. Isot.* **50**, 895 (1999).
8. M. R. McDevitt, R. D. Finn, D. Ma, S. M. Larson, D. A. Scheinberg, *J. Nucl. Med.* **40**, 1722 (1999).
9. M. W. Geerlings Sr., F. M. Kaspersen, C. Apostolidis, R. Van Der Hout, *Nucl. Med. Commun.* **14**, 121 (1993).
10. M. R. McDevitt *et al.*, *Eur. J. Nucl. Med.* **25**, 1341 (1998).
11. Supplementary material is available on *Science* Online at www.sciencemag.org/cgi/content/full/294/5546/1537/DC1.
12. The potency and specificity of [^{225}Ac]immunoglobulin G (IgG) for killing single cancer cells were determined using 2.5 × 10^3 to 5 × 10^4 cells (0.2 ml per well) in 96-well plates. Serial dilutions of [^{225}Ac]IgG were added to the cells to yield final activity in the wells ranging from 74 kBq/ml to 37 × 10^{-6} kBq/ml. Nonspecific killing was measured after target cells were blocked with a 100- to 10,000-fold excess of unlabeled IgG before plating and subsequent addition of [^{225}Ac]IgG. J591 is a murine IgG2A directed against prostate-specific membrane antigen (PSMA), expressed on LNCaP human prostate carcinoma cells; B4 is a murine IgG1 directed against CD19, expressed on human Ramos and Daudi lymphoma cells; HuM195 is a humanized IgG1 directed against CD33, expressed on human HL60 leukemia cells; 3F8 is a murine IgG3 directed against GD2 expressed on NMB7 human neuroblastoma cells; and Herceptin is a humanized IgG1 directed against HER2, expressed on human MCF7 breast carcinoma cells and SKOV3 ovarian carcinoma cells.
13. D. Ma *et al.*, *J. Nucl. Med.* **41**, 1175 (2000).
14. H. Liu *et al.*, *Cancer Res.* **58**, 4055 (1998).
15. P. M. Smith-Jones *et al.*, *Cancer Res.* **60**, 5237 (2000).
16. D. Ma *et al.*, *Leukemia*, in press.
17. J. M. Bidart *et al.*, *Clin. Chem.* **45**, 1695 (1999).
18. M. E. Gleave, J.-T. Hsieh, H.-C. Wu, A. C. von Eschenbach, W. K. Chung, *Cancer Res.* **52**, 1598 (1992).
19. In other experiments, the maximum tolerated dose (MTD) in 20 g mice was 18.5 kBq (500 nCi) [^{225}Ac]IgG. Mice injected with 37 kBq (1000 nCi) of [^{225}Ac]IgG died. On the basis of these studies, therapeutic doses were selected that were approximately 40% of MTD. Two normal male cynomolgus monkeys (*Macaca cynomolgus*) have been intravenously infused with a similar dose (based on weight) without toxicity.
20. M. A. Ghetie *et al.*, *Blood* **83**, 1329 (1994).
21. S. J. Kennel *et al.*, *Cancer Biother. Radiopharm.* **15**, 235 (2000).
22. I. A. Davis *et al.*, *Nucl. Med. Biol.* **26**, 581 (1999).
23. L. L. Chappell, K. A. Deal, E. Dadachova, M. W. Brechbiel, *Bioconjugate Chem.* **11**, 510 (2000).
24. K. A. Deal, I. A. Davis, S. Mirzadeh, S. J. Kennel, M. W. Brechbiel, *J. Med. Chem.* **42**, 2988 (1999).

25. Supported by NIH grants RO1 CA55349 and PO1 33049, the CaPCure Foundation, the Lymphoma Foundation, the Cure For Lymphoma Foundation, the Gabrielle Rich Foundation, the Doris Duke Charitable Foundation, and the Pepsico Foundation. We thank M. Geerlings Sr. for helpful discussions.

5 July 2001; accepted 27 September 2001

Induction of Dendritic Cell Differentiation by IFN-α in Systemic Lupus Erythematosus

Patrick Blanco,[1]* A. Karolina Palucka,[1]* Michelle Gill,[1,2] Virginia Pascual,[1,2] Jacques Banchereau[1]†

Dendritic cells (DCs) are important in regulating both immunity and tolerance. Hence, we hypothesized that systemic lupus erythematosus (SLE), an autoimmune disease characterized by autoreactive B and T cells, may be caused by alterations in the functions of DCs. Consistent with this, monocytes from SLE patients' blood were found to function as antigen-presenting cells, in vitro. Furthermore, serum from SLE patients induced normal monocytes to differentiate into DCs. These DCs could capture antigens from dying cells and present them to CD4-positive T cells. The capacity of SLE patients' serum to induce DC differentiation correlated with disease activity and depended on the actions of interferon-α (IFN-α). Thus, unabated induction of DCs by IFN-α may drive the autoimmune response in SLE.

Lupus (SLE) is a systemic autoimmune disease characterized by a waxing and waning course and the involvement of multiple organs, including skin, kidneys, and central nervous system (*1*). Although SLE etiopathology is poorly understood, there is likely a role for environmental triggers, for instance viruses, acting in the context of susceptibility genes (*2*, *3*). Now, SLE therapy is based on nonspecific immunosuppression and symptom control; however, no cure for SLE has been found, and that is particularly needed for children, whose disease often progresses to chronic renal failure and/or death (*1*). Among the immunological features of SLE are high titers of autoantibodies predominantly specific for DNA and nucleosomes (*4*, *5*). Paradoxically, polyclonal hypergammaglobulinemia, high plasma cell numbers, and an increased frequency of pre–germinal center B cells (*6*, *7*) coincide with considerable B lymphopenia. Likewise, autoreactive T cells are found in the blood despite T lymphopenia (*8*, *9*). The systemic autoimmune response that characterizes SLE might be explained by alter-

[1]Baylor Institute for Immunology Research, Dallas, TX 75204, USA. [2]The University of Texas Southwestern Medical Center at Dallas, Dallas, TX 75390, USA.

*These authors contributed equally to this work.
†To whom correspondence should be addressed. E-mail: j.banchereau@baylordallas.edu